Thermoelectric figure of merit of $(In_{0.53}Ga_{0.47}As)_{0.8}(In_{0.52}Al_{0.48}As)_{0.2}$ III-V semiconductor alloys

Je-Hyeong Bahk,[1] Zhixi Bian,[2] Mona Zebarjadi,[2] Joshua M. O. Zide,[3] Hong Lu,[1,4] Dongyan Xu,[5] Joseph P. Feser,[5] Gehong Zeng,[1] Arun Majumdar,[5] Arthur C. Gossard,[4] Ali Shakouri,[2] and John E. Bowers[1]

[1]*Department of Electrical and Computer Engineering, University of California, Santa Barbara, California 93106, USA*

[2]*Electrical Engineering Department, University of California, Santa Cruz, California 95064, USA*

[3]*Materials Science and Engineering Department, University of Delaware, Newark, Delaware 19716, USA*

[4]*Materials Department, University of California, Santa Barbara, California 93106, USA*

[5]*Department of Mechanical Engineering, University of California, Berkeley, California 94720, USA*

(Received 9 February 2010; revised manuscript received 15 April 2010; published 10 June 2010)

The thermoelectric figure of merit is measured and theoretically analyzed for *n*-type Si-doped InGaAlAs III-V quaternary alloys at high temperatures. The Seebeck coefficient, electrical conductivity, and thermal conductivity of a Si-doped $(In_{0.53}Ga_{0.47}As)_{0.8}(In_{0.52}Al_{0.48}As)_{0.2}$ of 2 μm thickness lattice matched to InP substrate grown by molecular-beam epitaxy are measured up to 800 K. The measurement results are analyzed using the Boltzmann transport theory based on the relaxation-time approximation and the theoretical calculation is extended to find optimal carrier densities that maximize the figure of merit at various temperatures. The figure of merit of 0.9 at 800 K is measured at a doping level of 1.9×10^{18} cm^{-3} and the theoretical prediction shows that the figure of merit can reach 1.3 at 1000 K at a doping level of 1.5×10^{18} cm^{-3}.

DOI: 10.1103/PhysRevB.81.235209 PACS number(s): 84.60.Rb, 73.50.Lw, 73.61.Ey

I. INTRODUCTION

Seeking a better thermoelectric material for efficient thermal-to-electrical energy conversion has become more important as energy efficiency becomes an increasing critical issue.[1] The efficiency of a thermoelectric material is directly linked to the dimensionless thermoelectric figure of merit, $ZT=S^2\sigma T/\kappa$, where S, σ, T, and κ are, respectively, the Seebeck coefficient, electrical conductivity, temperature, and thermal conductivity. III-V compound semiconductors are promising thermoelectric materials because they offer several advantages such as high mobility, reduced thermal conductivity by alloying, and established pathways toward composing low-dimensional structures and nanocomposites.[2–6]

In early research on III-V semiconductors for thermoelectric applications, narrow band-gap materials with light electron effective masses such as InAs and InSb were studied because of their relatively high *ZT*'s with high electron mobility.[7,8] Recently Mingo calculated the figure of merits of various nanowires (NWs) made of III-V semiconductors based on the exact solution of the Boltzmann transport equation and predicted that *ZT* can be much higher than unity at room temperature for ultrathin NWs such as InSb NWs thinner than 15 nm and InAs NWs thinner than 5 nm in diameter.[9] The InSb and InAs nanowires have been successfully grown by vapor-liquid-solid process,[2,3] and as uniform arrays by chemical-beam epitaxy,[4] respectively. Wide band-gap III-V semiconductors such as GaN and InGaN have also attracted increased attention recently for thermoelectric power generation as candidates to substitute SiGe in high-temperature applications because they are nontoxic, very stable at high temperatures, and can be easily integrated with the devices made of GaN or related materials.[10,11]

Recently it has been reported that ErAs nanoparticles of 2–3 nm in diameter can be epitaxially embedded within III-V semiconductors during the growth by molecular-beam epitaxy.[5,6] Kim *et al.*[12] showed that the ErAs:InGaAs semimetal/semiconductor nanocomposites could effectively reduce the thermal conductivity further below the alloy limit. Zebarjadi *et al.*[13] also showed that the ErAs nanoparticles could enhance the thermoelectric power factor ($S^2\sigma$) as well in the semiconductor matrix of InGaAlAs through an energy-dependent electron scattering in specific conditions. For a detailed investigation on the nanostructured material, however, it is essential to first fully understand the electron and thermoelectric transport behavior in the semiconductor matrix without nanoparticles. Mobility calculations for the ternary and quaternary alloys have been performed in previous papers.[14–16] However, those results showed the data only at room temperature or lower temperatures.

In this paper, we present an experimental and theoretical investigation on the thermoelectric figure of merit of the Si-doped $(In_{0.53}Ga_{0.47}As)_{0.8}(In_{0.52}Al_{0.48}As)_{0.2}$ quaternary alloy based on the high-temperature measurements of electrical conductivity, Seebeck coefficient, and thermal conductivity performed up to 800 K. Temperature-dependent Hall effect measurements are also performed on the material to find the Hall mobility from 40 to 400 K. The Hall mobility data is fitted with theoretical calculation by solving the Boltzmann transport equation in the relaxation-time approximation. The calculated mobility is then used to estimate the electrical conductivity and Seebeck coefficient for comparison with the experimental results. The electronic thermal conductivity is also calculated using the electron-transport characteristics. The lattice thermal conductivity, which is independent of the doping level, is extracted by subtracting the electronic component from the total thermal conductivity measured. The optimal carrier density that maximizes the *ZT* at a given temperature is calculated using the developed theoretical model at various temperatures up to 1000 K.

II. ELECTRON TRANSPORT IN III-V SEMICONDUCTOR ALLOYS

In the III-V semiconductor alloys, the conduction-band minimum is located at the Γ valley with spherical constant

energy surface. We assume a single band model in this paper as the minimum of the second lowest L valley is located much higher than the Fermi level of our interest. The dispersion relation is described by the Kane model,[17]

$$E(1+\alpha E)=\frac{\hbar^2k^2}{2m^*}, \tag{1}$$

where α is nonparabolicity and m^* is the effective mass at the conduction-band minimum.

Electron transport and thermoelectric properties can be derived from the Boltzmann transport equation with the relaxation-time approximation. They are all integral functions of the differential conductivity,[18,19]

$$\sigma_d(E)=e^2\tau(E)v^2(E)\rho_{DOS}(E)\left(-\frac{\partial f_0}{\partial E}\right), \tag{2}$$

where $\tau(E)$ is the total electron relaxation time, $v(E)$ is the electron velocity in one direction, $\rho_{DOS}(E)$ is the density of states, and $f_0(E)$ is the Fermi-Dirac distribution.

The total electron relaxation time is determined by relevant electron-scattering mechanisms. Dominant scattering mechanisms in III-V semiconductor alloys are polar optical-phonon (POP) scattering, ionized impurity (II) scattering, alloy scattering, and acoustic-phonon deformation-potential scattering.[15–17] The acoustic-phonon deformation-potential scattering is usually weak but becomes strong at high temperatures. Thus, the total relaxation time for III-V semiconductor alloys is given by

$$\frac{1}{\tau(E)}=\frac{1}{\tau_{\mathrm{POP}}(E)}+\frac{1}{\tau_{\mathrm{II}}(E)}+\frac{1}{\tau_{AL}(E)}+\frac{1}{\tau_{AC}(E)}, \tag{3}$$

where $\tau_{\mathrm{POP}}(E)$, $\tau_{\mathrm{II}}(E)$, $\tau_{AL}(E)$, and $\tau_{AC}(E)$ are, respectively, the polar optical-phonon scattering time,[17] the ionized impurity scattering time,[20] the alloy scattering time,[21] and the acoustic-phonon deformation-potential scattering time.[17] The ionized impurity scattering time is inversely proportional to carrier concentration.

The electrical conductivity σ is simply an integral of the differential conductivity over energy, and the mobility μ is related to the electrical conductivity by $\sigma=ne\mu$, where n is the carrier concentration,

$$\sigma=F_0(E_F), \tag{4}$$

$$\mu=\frac{1}{e}\frac{F_0(E_F)}{\int_0^\infty \rho_{DOS}(E)f_0(E)dE}, \tag{5}$$

where E_F is the Fermi level relative to the conduction-band minimum, and

$$F_m(E_F)=\int_0^\infty \sigma_d(E)(E-E_F)^m dE.$$

The Seebeck coefficient is given by[22]

$$S=\frac{1}{eT}\frac{F_1(E_F)}{F_0(E_F)}. \tag{6}$$

If the carrier concentration is increased, the mobility is reduced by the increased ionized impurity scattering. However, increased carrier concentration outweighs decreased mobility so that the electrical conductivity always increases with increasing carrier concentration. On the other hand, the Seebeck coefficient is decreased by increasing carrier concentration.

The electronic component of thermal conductivity is given by[22]

$$\kappa_e=\frac{1}{e^2T}\left\{F_2(E_F)-\frac{[F_1(E_F)]^2}{F_0(E_F)}\right\}. \tag{7}$$

It is convenient to describe the electronic component of thermal conductivity with the Lorenz number defined as $L=\kappa_e/(\sigma T)$. From Eqs. (4) and (7), the Lorenz number is derived as

$$L=\frac{1}{e^2T^2}\left\{\frac{F_2(E_F)}{F_0(E_F)}-\frac{[F_1(E_F)]^2}{[F_0(E_F)]^2}\right\}. \tag{8}$$

The Lorenz number is a constant, $L_0=(\pi k_B)^2/3e^2\approx 2.44\times 10^{-8}$ W Ω K^{-2}, for metals or in the degenerate limit ($E_F \gg 0$) according to the Wiedemann-Franz law.[23] In semiconductors, however, the Lorenz number is reduced from L_0, and results in a reduction of the electronic contribution to thermal conductivity.

III. EXPERIMENTS

The 1.9×10^{18} cm^{-3} Si-doped $(In_{0.53}Ga_{0.47}As)_{0.8}(In_{0.52}Al_{0.48}As)_{0.2}$ thin films of 2 μm thickness were grown on 2 in. lattice-matched InP substrate wafers using digital alloy growth technique by molecular-beam epitaxy at a growth temperature of 490 °C. The InP substrate that the epitaxial film was grown on was doped by deep level Fe dopants to compensate the intrinsic carriers and thus is semi-insulating at room temperature. However, the thermal excitation of free carriers in the substrate increases exponentially with temperature and affects the electrical measurements of the thin film at high temperatures above 600 K. To eliminate the substrate effect, we bonded the III-V thin film onto an insulating sapphire substrate using an oxide bonding technique, and the original InP substrate was then removed by selective wet etching, leaving only the thin film on the sapphire.[24]

A cloverleaf-shaped van der Pauw pattern was fabricated on the transferred thin film on a sapphire substrate for electrical conductivity and Hall effect measurements[25] with subsequent surface passivation using multiple layer deposition of the plasma-enhanced chemical-vapor deposition SiN_x and SiO_2 on the thin film to prevent the epitaxial layer from decomposing at temperatures higher than the growth temperature. The same sample was used for Seebeck measurements by measuring voltage across the two metal contacts in a diagonal direction with temperature gradient. For comparison, another sample on the original InP substrate cleaved

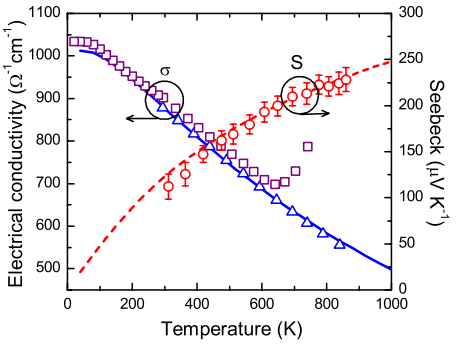

FIG. 1. (Color online) Electrical conductivity and Seebeck coefficient vs temperature for the Si-doped $(In_{0.53}Ga_{0.47}As)_{0.8}(In_{0.52}Al_{0.48}As)_{0.2}$. Electrical conductivity measured on both the original InP substrate (squares) and a sapphire substrate (triangles). Seebeck coefficients measured on a sapphire substrate (circles). The solid and dotted lines are theoretical calculations for electrical conductivity and Seebeck coefficient, respectively.

from the same wafer was also processed following the same processing steps except the substrate removal and oxide bonding.

Thermal conductivity was measured using the 3ω method.[12] The substrate was not removed for the thermal-conductivity measurements because the thermal conductivity contrast between the substrate and the epitaxial film is sufficiently large in the measurement temperature range so that they can be easily separated.

IV. RESULTS AND DISCUSSION

Figure 1 shows the measurement results of the electrical conductivity and Seebeck coefficient of the thin-film Si-doped $(In_{0.53}Ga_{0.47}As)_{0.8}(In_{0.52}Al_{0.48}As)_{0.2}$. Both the electrical conductivities measured on the original InP substrate and on the sapphire substrate after the InP substrate removal are shown in Fig. 1 for comparison. The former shows a sudden increase above 650 K, while the latter shows no such an increase, but a steady decrease in electrical conductivity, which is a clear evidence that the substrate conduction through the InP substrate showed up in the original sample above 650 K, but has been removed in the substrate-removed sample. The small discrepancy in electrical conductivity between the two samples below 650 K can be due to the strain effect induced on the thin films by the different degree of thermal-expansion mismatch with the two dissimilar substrates or slight difference in doping density between the two samples originating from doping nonuniformity on the wafer. The Seebeck coefficient measured for the substrate-removed sample is also shown in Fig. 1 and good agreement with the theoretical calculation is observed.

The electrical conductivity measured for the thin film on the sapphire substrate was fitted theoretically in Fig. 1 using the four scattering mechanisms in the III-V alloys. Table I shows the material properties used to calculate the scattering rates and transport properties of the $(In_{0.53}Ga_{0.47}As)_{0.8}(In_{0.52}Al_{0.48}As)_{0.2}$ lattice matched to the InP substrate. Two fitting parameters were used for the fitting of the total mobility, one of which is the alloy scattering potential and the other is the carrier compensation ratio defined as the ratio of the density of ionized impurities to the actual carrier density. The alloy scattering potential used for the final fitting is 0.32 ± 0.01 eV, which is close to the electron negativity difference, 0.33 eV, calculated for the quaternary compound using the formulas given in Ref. 30. The compensation ratio was determined to be 1.22, which is reasonably low compared to 1.67 used in Ref. 15. Figure 2 shows the Hall mobility fitting with the four relevant scattering mechanisms. The mobility of each scattering mechanism in Fig. 2, which shows the relative strength of each scattering, was calculated by plugging the relaxation time of the specific scattering mechanism into Eq. (5) instead of the total relaxation time. The carrier density was measured by the Hall effect measurement and was almost constant, 1.9×10^{18} cm^{-3}, from 40 to 400 K, and is expected to remain almost the same up to 1000 K with the fact that intrinsic carrier density is still sufficiently low below 10^{17} cm^{-3} in the temperature range.

TABLE I. Material properties used in the transport calculation for $(InGaAs)_{0.8}(InAlAs)_{0.2}$ lattice matched to InP. The last two parameters were used as adjustable parameters for fitting the Hall mobility data.

Electron effective mass	$0.0478m_0$ (Ref. 26)
Nonparabolicity	1.102 (1/eV) (Ref. 26)
Static dielectric constant	13.6 (Ref. 16)
High-frequency dielectric constant	11.5 (Ref. 16)
Optical-phonon energy	0.032 (eV) (Ref. 27)
Acoustic deformation potential	5.92 (eV) (Ref. 28)
Elastic constant	1.02×10^{11} (N/m^2) (Ref. 29)
Alloy scattering potential	0.32 (eV)
Carrier compensation ratio	1.22

Figure 3 shows both the lattice component and the electronic component of thermal conductivity along with the measured total thermal conductivity. The calculation of lattice thermal conductivity is beyond this work. Instead, it was extracted from the measurement data of the total thermal

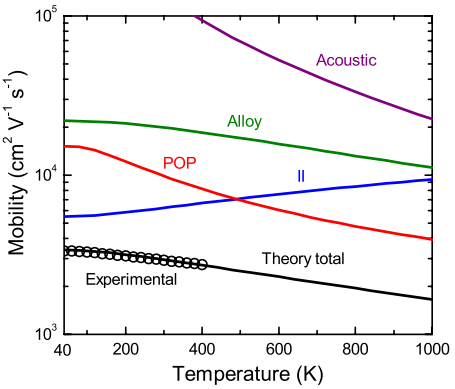

FIG. 2. (Color online) Mobility fitting for the Si-doped $(In_{0.53}Ga_{0.47}As)_{0.8}(In_{0.52}Al_{0.48}As)_{0.2}$. Alloy, POP, II, and acoustic-phonon scatterings are included. Experimental data measured from 40 to 400 K is designated by open circles.

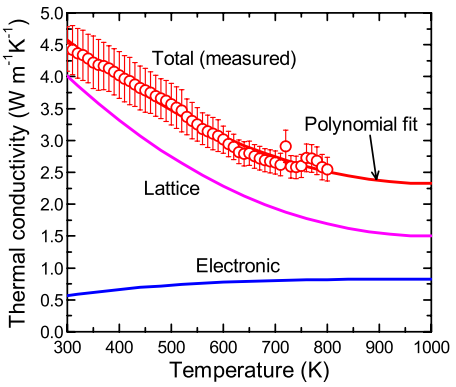

FIG. 3. (Color online) Thermal conductivity vs temperature for the Si-doped $(In_{0.53}Ga_{0.47}As)_{0.8}(In_{0.52}Al_{0.48}As)_{0.2}$. The measured thermal conductivity is shown in open circles with a quadratic polynomial fitting in a solid line. The electronic component of thermal conductivity (the bottom curve) is calculated from the electron scattering characteristics, and the lattice thermal conductivity curve shown in the middle is the difference between the fitting curve of the measured data and the electronic thermal conductivity.

conductivity by subtracting the calculated electronic thermal conductivity. The electronic thermal conductivity steadily increases with temperature, but the increase is slower as temperature goes up, and finally it saturates above 700 K because both the electrical conductivity and the Lorenz number keep decreasing with temperature. The Lorenz number and the Fermi level are shown as a function of temperature in Fig. 4. As the Fermi level decreases with increasing temperature, the semiconductor deviates further from the Wiedemann-Franz law, which results in the reduction in the Lorenz number.[23] The saturated electronic thermal conductivity at high temperatures is another advantage of this material for keeping the total thermal conductivity low and the figure of merit high. The lattice thermal conductivity is also reduced in the high-temperature region mainly due to the umklapp scattering.[12] The low lattice thermal conductivity can also be attributed partly to the digital alloy growth in which the periodic interfaces in monolayer scale can still scatter phonons to reduce lattice thermal conductivity.

Figure 5 shows the measured power factor and the figure of merit along with their theoretical calculations as functions

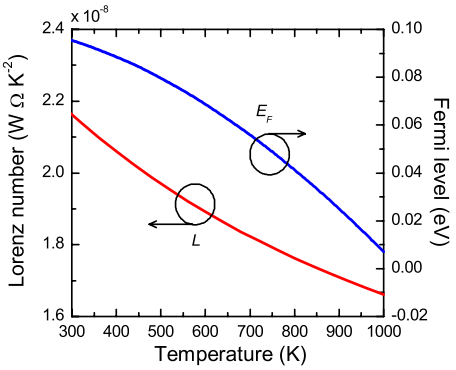

FIG. 4. (Color online) Calculated Lorenz number (L) and Fermi level (E_F) vs temperature for the Si-doped $(In_{0.53}Ga_{0.47}As)_{0.8}(In_{0.52}Al_{0.48}As)_{0.2}$.

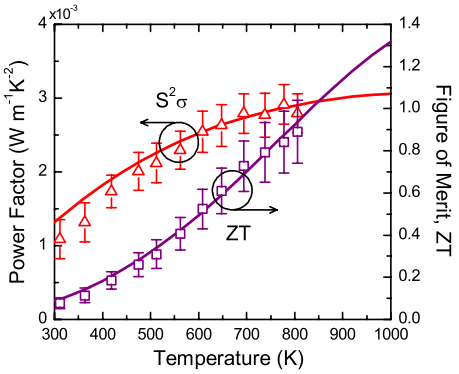

FIG. 5. (Color online) Power factor ($S^2\sigma$), and the figure of merit, ZT, of the 1.9×10^{18} cm^{-3} Si-doped $(In_{0.53}Ga_{0.47}As)_{0.8}(In_{0.52}Al_{0.48}As)_{0.2}$ as a function of temperature, in which the experimental results are shown as open triangles and squares, respectively. The solid curves are theoretical calculations.

of temperature for the material at a doping level of 1.9×10^{18} cm^{-3}. The figure of merit was measured to be 0.9 at 800 K and is expected to keep increasing with temperature to reach 1.3 at 1000 K according to the theoretical calculation. Figure 6 shows doping density dependence of the thermoelectric properties calculated based on the measured data at a doping level of 1.9×10^{18} cm^{-3} at 800 K. As doping density increases, the electrical conductivity increases while the Seebeck coefficient decreases, and their trade-off relation makes a peak in power factor in the middle of the doping density around 3×10^{18} cm^{-3}. However, the thermal conductivity also increases with increasing doping density because its electronic component increases with doping density almost linearly and becomes a dominant factor over the lattice component at high doping levels. For example, the increasing rate of electronic thermal conductivity is calculated to be around 0.4 W/m K per 1×10^{18} cm^{-3} increase in doping density at 800 K. The lattice thermal conductivity is kept constant with varying doping density. Because of the increased thermal conductivity, the ZT drops more quickly than the power factor as the doping density increases, so that ZT has a peak at a slightly lower doping of 1.3×10^{18} cm^{-3}.

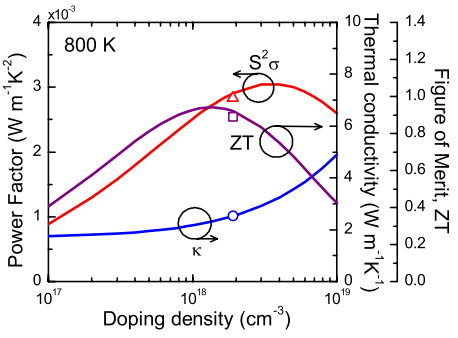

FIG. 6. (Color online) Theoretical calculations of the power factor ($S^2\sigma$), thermal conductivity (κ), and the figure of merit, ZT, of the Si-doped $(In_{0.53}Ga_{0.47}As)_{0.8}(In_{0.52}Al_{0.48}As)_{0.2}$ as functions of doping density at 800 K. The measured values at a doping density of 1.9×10^{18} cm^{-3} are also shown as a triangle, a circle, and a square, respectively.

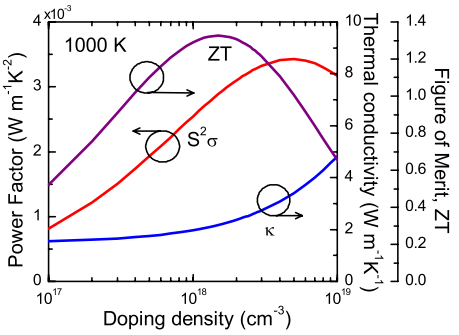

FIG. 7. (Color online) Theoretical calculations of the power factor ($S^2\sigma$), thermal conductivity (κ), and the figure of merit, ZT, of the Si-doped $(In_{0.53}Ga_{0.47}As)_{0.8}(In_{0.52}Al_{0.48}As)_{0.2}$ as functions of doping density at 1000 K.

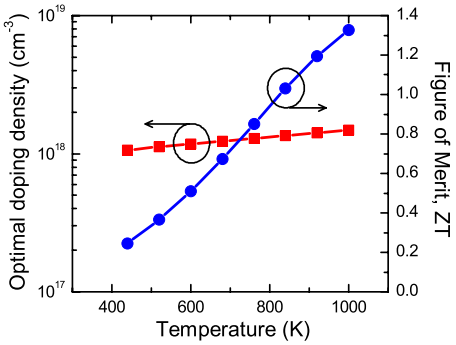

FIG. 8. (Color online) Optimal doping densities at various temperatures that maximize the figure of merit and the maximum values of the figure of merit.

In Fig. 7, the theory has been extended to calculate the thermoelectric properties at 1000 K as functions of doping density. The ZT has a peak at around 1.5×10^{18} cm^{-3}, and the maximum ZT is found to be 1.3 at 1000 K. The ZT enhancement from 800 to 1000 K is mainly due to the temperature increase and the slight enhancement of power factor. As shown in Fig. 8, the optimal doping density that maximizes the figure of merit at a given temperature does not change much with temperature, ranging between 1×10^{18} -1.5×10^{18} cm^{-3}, slightly increasing with temperature. The corresponding maximum figure of merit, however, rapidly increases with temperature due to the enhanced power factor and reduced thermal conductivity along with the multiplication of the increased temperature. Beyond 1000 K, the intrinsic carriers by thermal excitation may not be negligible in the carrier transport so that the increase in the figure of merit can be suppressed.

V. CONCLUSIONS

We have experimentally measured the figure of merit of Si-doped $(In_{0.53}Ga_{0.47}As)_{0.8}(In_{0.52}Al_{0.48}As)_{0.2}$ lattice matched to the InP substrate grown by molecular-beam epitaxy from room temperature and fit the measurement results using the solution of the Boltzmann transport equation in the relaxation-time approximation. The ZT of 0.9 at 800 K was measured for this material. By extracting the adjustable parameters from the fitting of the measurements, we have extended the theory to predict the thermoelectric properties of the material at various doping levels and temperatures higher than the measurement limit. It has been predicted that the ZT can be 1.3 at 1000 K at a doping level of 1.5×10^{18} cm^{-3}. The power factor steadily increases with temperature in this temperature range and the saturated electronic thermal conductivity helps to maintain the ZT high at high temperatures.

ACKNOWLEDGMENTS

The authors are grateful to Ashok Ramu and Peter Burke for their very helpful discussion. This work was supported by the ONR MURI Thermionic Energy Conversion Center, and the DARPA Nanostructured Material for Power (NMP) program.

[1] G. J. Snyder and E. S. Toberer, Nature Mater. **7**, 105 (2008).
[2] Q. L. Ye, T. Yamada, H. Liu, R. Scheffler, N. Mingo, and R. Leverenz, *Semiconductor Nanowires – Fabrication, Physical Properties, and Applications*, edited by V. Schmidt (MRS Symposia Proceedings No. 940E (Materials Research Society, Warrendale, PA, 2006), p. P07-05.
[3] H. D. Park, S. M. Prokes, M. E. Twigg, Y. Ding, and Z. L. Wang, J. Cryst. Growth **304**, 399 (2007).
[4] A. I. Persson, L. E. Fröberg, L. Samuelson, and H. Linke, Nanotechnology **20**, 225304 (2009).
[5] D. C. Driscoll, M. P. Hanson, E. Mueller, and A. C. Gossard, J. Cryst. Growth **251**, 243 (2003).
[6] D. O. Klenov, D. C. Driscoll, A. C. Gossard, and S. Stemmer, Appl. Phys. Lett. **86**, 111912 (2005).
[7] R. Bowers, R. W. Ure, J. E. Bauerle, and A. J. Cornish, J. Appl. Phys. **30**, 930 (1959).
[8] D. L. Rode, Phys. Rev. B **3**, 3287 (1971).
[9] N. Mingo, Appl. Phys. Lett. **84**, 2652 (2004); **88**, 149902 (2006) (erratum).
[10] B. N. Pantha, R. Dahal, J. Li, J. Y. Lin, H. X. Jianga, and G. Pomrenke, Appl. Phys. Lett. **92**, 042112 (2008).
[11] A. Sztein, H. Ohta, J. Sonoda, A. Ramu, J. E. Bowers, S. P. DenBaars, and S. Nakamura, Appl. Phys. Express **2**, 111003 (2009).
[12] W. Kim, J. Zide, A. Gossard, D. Klenov, S. Stemmer, A. Shakouri, and A. Majumdar, Phys. Rev. Lett. **96**, 045901 (2006).
[13] M. Zebarjadi, K. Esfarjani, A. Shakouri, J.-H. Bahk, Z. Bian, G. Zeng, J. Bowers, H. Lu, J. Zide, and A. Gossard, Appl. Phys. Lett. **94**, 202105 (2009).
[14] J. D. Oliver, L. F. Eastman, P. D. Kirchner, and W. J. Schaff, J. Cryst. Growth **54**, 64 (1981).
[15] Y. Takeda, M. A. Littlejohn, and J. R. Hauser, Electron. Lett. **17**, 377 (1981).
[16] S. Adachi, *Physical Properties of III-V Semiconductor Compounds: InP, InAs, GaAs, GaP, InGaAs, and InGaAsP* (Wiley-Interscience, New York, 1992).

[17] M. Lundstrom, *Fundamentals of Carrier Transport*, 2nd ed. (Cambridge University Press, Cambridge, England, 2000).
[18] G. S. Nolas, J. Sharp, and H. J. Goldsmid, *Thermoelectrics: Basic Principles and New Materials Developments* (Springer-Verlag, Berlin, 2001).
[19] A. Shakouri, E. Y. Lee, D. L. Smith, V. Narayanamurti, and J. E. Bowers, Nanosc. Microsc. Therm. **2**, 37 (1998).
[20] H. Brooks, Adv. Electron. Electron Phys. **7**, 85 (1955).
[21] J. W. Harrison and J. R. Hauser, Phys. Rev. B **13**, 5347 (1976).
[22] N. W. Ashcroft and N. D. Mermin, *Solid State Physics* (Holt, Rinehart, and Winston, New York, 1976), Chap. 13.
[23] J. R. Drabble and H. J. Goldsmid, *Thermal Conduction in Semiconductors* (Pergamon, New York, 1961).
[24] J.-H. Bahk, G. Zeng, J. M. O. Zide, H. Lu, R. Singh, D. Liang, A. T. Ramu, Z. Bian, A. Shakouri, A. C. Gossard, and J. E. Bowers, J. Electron. Mater. (to be published).
[25] L. J. Van der Pauw, Philips Res. Rep. **13**, 1 (1958).
[26] *Semiconductors-Group IV Elements, IV-IV and III-V Compounds*, Landolt-Börnstein New Series, Group III: Condensed Matter Vol. 41A1b, edited by H. Rössler (Springer, Heidelberg, 2002).
[27] R. Borroff, R. Merlin, A. Chin, and P. K. Bhattacharya, Appl. Phys. Lett. **53**, 1652 (1988).
[28] I. Vurgaftman, J. R. Meyer, and L. R. Ram-Mohan, J. Appl. Phys. **89**, 5815 (2001).
[29] C. G. Van de Walle, Phys. Rev. B **39**, 1871 (1989).
[30] M. A. Littlejohn, J. R. Hauser, and T. H. Glisson, Solid-State Electron. **21**, 107 (1978).